A responsive MRI contrast agent for detection of excess copper(II) in the liver *in vivo*

Namini N. Paranawithana,[1] Andre F. Martins,[1] Veronica Clavijo-Jordan,[2] Piyu Zhao,[1] Sara Chirayil,[2] Gabriele Meloni[1] and A. Dean Sherry[1,2]*

[1]Department of Chemistry and Biochemistry, University of Texas at Dallas, Richardson, Texas, USA.

[2]Advanced Imaging Research Center, University of Texas Southwestern Medical Center, Dallas, Texas, USA.

Contents

Materials and Methods

$DO3A\text{-}tBu_3$ was synthesized according to the reported procedure in literature[1]. Chemicals were purchased from Sigma–Aldrich (St. Louis, MO), Strem (Newburyport, M), Acros Organics (Morris Plains, NJ), TCI America (Portland, OR), and Alfa Aesar (Ward Hill, MA). They were used as received unless otherwise noted. Human Serum Albumin (HSA, fatty acid and globulin free) was purchased from Sigma-Aldrich. Column chromatography was performed using Silica gel (200-400 mesh, 60A°), purchased from Sigma-Aldrich. Analytical Thin Layer Chromatography was performed using EMD Millipore precoated aluminum oxide or Whatman precoated Silica gel on a polyester plate. Analytical HPLC was performed on an Agilent Technologies 1220 Infinity LC using a RESTEK Ultra C-18 IBD column (3 μm, 100 × 4.6 mm). Preparative HPLC was performed on a Waters Delta Prep HPLC system equipped with a Water® 2996 photodiode array detector and a Phenomenex Kinetex® C18 column (5 μm, 21.2 mm x 250 mm) or an Atlantis Prep T3 OBD Column (5 μm, 30 mm x 250 mm). A Fisher Science Education pH-meter coupled with Thermo Scientific Orion Micro pH electrode was used for pH measurements. Milli-Q purified water was used for the preparation of all samples and preparative and analytical HPLC. ^{1}H and ^{13}C NMR spectra were obtained in deuterated solvents from Cambridge Isotope Laboratories (Cambridge, MA) on a Bruker AVANCE III 400 MHz NMR spectrometer for all synthetic intermediates, final products, ^{17}O temperature studies of all lanthanide complexes. A VirTis Freeze Dryer (Benchtop-k) was used to lyophilize the samples. Mass spectra were obtained using either HT Laboratories (San Diego, CA) instrument or a Waters Alliance e2695 Separations Module coupled with Xevo QTof MS using an Atlantis T3 Column (5 μm, 6 mm x 250 mm) at The Advanced Imaging Research Center (University of Texas Southwestern Medical Center, Dallas). Inductive coupled plasma mass spectrometry (ICP-MS) was performed for calculating metal concentrations using Agilent 7900. Standard solutions for ICP-MS containing Gd, Eu, La, and Yb were purchased from Inorganic Ventures (Christiansburg, VA). Florescence Measurements were collected in Horiba Fluoromax 4 (Albany, NY) spectrofluorometer. Electronic Paramagnetic Resonance spectroscopy was performed in Bruker EMX Spectrometer with ER 041 XG microwave bridge. Chemical structures and IUPAC names were obtained using Chemaxon MarvinSketch 17.11 and ChemdrawUltra 7.0.[2]

1. Synthesis

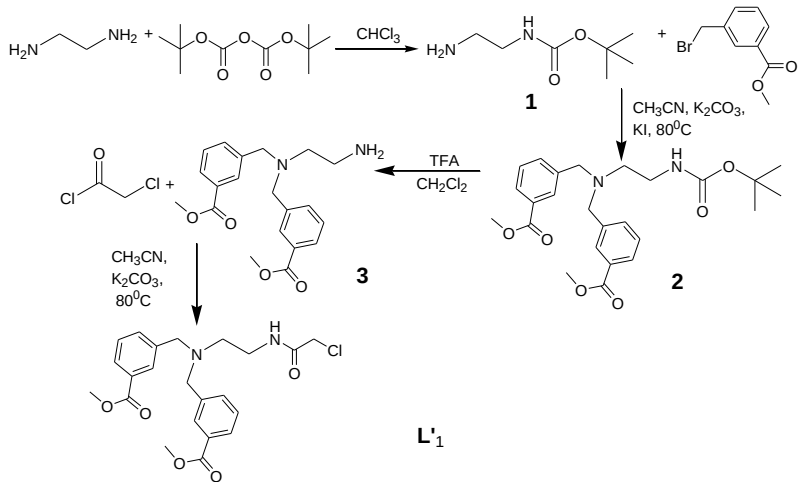

Scheme 1. Synthesis of L'_1.

methyl 3-(((2-((chloroacetyl)amino)ethyl)(3-(methoxycarbonyl)benzyl)amino)methyl)benzoate (L'_1)

Synthetic procedure for compound **1** was reported previously.[3] 1.0 g of Compound 1 (6.25 mmol) was added to 3-Bromomethyl benzoic acid (3.0 g, 13.8 mmol)) dissolved in acetonitrile (CH_3CN) with potassium carbonate (3.45 g, 25.0 mmol) and potassium iodide (0.5 g, 3.0 mmol), increased solvent volume up to 250 ml. The reaction mixture was refluxed for 18 hrs. The reaction mixture was filtered, the solvent was removed in vacuo. The residue was dissolved in dichloromethane and purified with a SiO_2 column using dichloromethane and methanol (R_f =0.65) to obtain compound **2**. Compound **2** (2.3 g, 5.0 mmol) was dissolved in CH_2Cl_2 (5ml) and TFA (10.5 ml) and kept at room temperature for 16 hrs to obtain compound **3**. Compound **3** (1.6 g, 4.5 mmol) was added to chloroacetyl chloride (0.6 ml, 6.25mmol) potassium carbonate (3.0 g, 22.0 mmol) dissolved in acetonitrile. The mixture was refluxed for 72 hrs, followed by filtration and solvent was removed by rotary evaporation to obtain the residue. The residue was dissolved and purified with SiO_2 by CH_2Cl_2 and CH_3OH) (60:40) (R_f = 0.75) to obtain L'_1 (2.2 g, 5.0 mmol, 80% yield).

^{1}H NMR (400 MHz, $CDCl_3$, TMS): δ 2.62 (2H, s, $CH_2NC\underline{H_2}CH_2N$), 3.32 (2H, s, $CH_2NCH_2C\underline{H_2}N$), 3.64 (4H, s. $PhC\underline{H_2}N$), 3.86 (6H, s, $C\underline{H_3}OCOPh$), 4.12 (2H, s, $NCOC\underline{H_2}Cl$), 7.39 (8H, s, $\underline{H}Ph$)

^{13}C NMR (400 MHz, $CDCl_3$, TMS): δ 37.05 ($NCH_2\underline{C}H_2N$), 42.57 ($NCO\underline{C}H_2Cl$), 51.99 ($\underline{C}H_3OCOPh$), 53.83 ($N\underline{C}H_2CH_2NHCO$), 58.14 ($Ph\underline{C}H_2NCH_2$), 128.55 ($Ph\underline{C}$), 166.84 ($CH_3O\underline{C}OPh$)

MS(ESI-positive) m/z = 432.46 [M-H$^+$] (calculated 432.20)

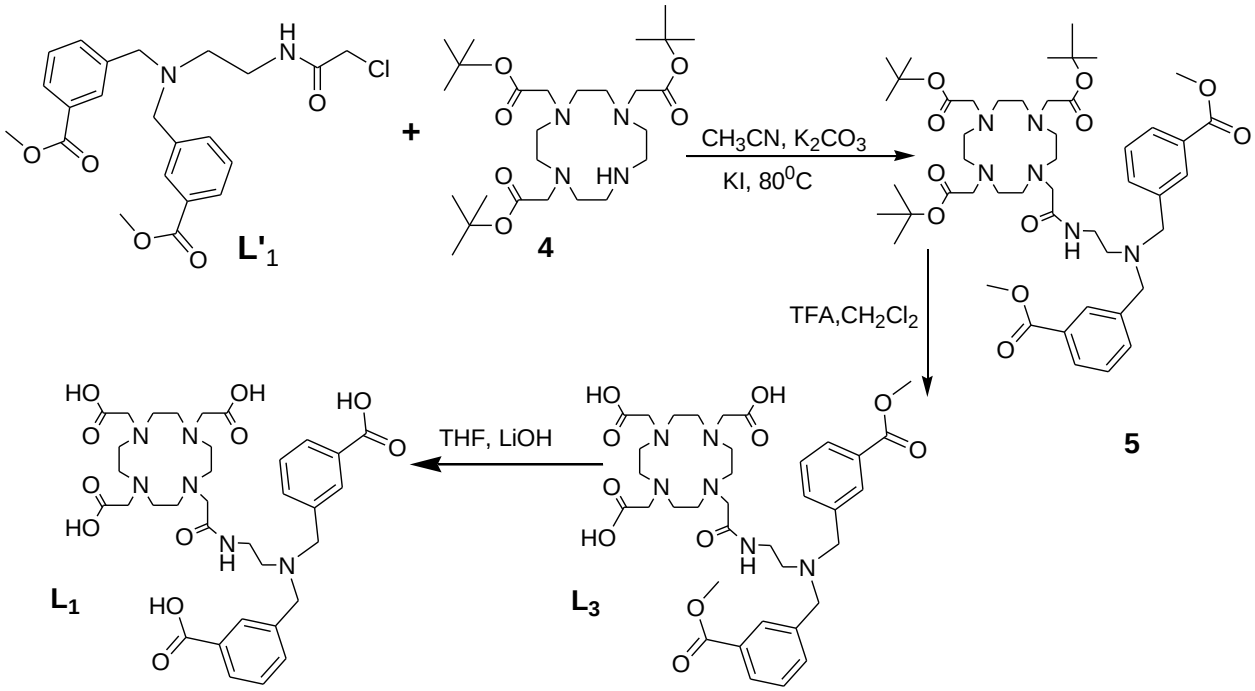

Scheme 2. Synthesis of L1.

3-(((2-(((4,7-bis(carboxymethyl)-10-(3-hydroxy-2-oxopropyl)-1,4,7,10-tetraazacyclododecan-1-yl)acetyl)amino)ethyl)(3-carboxybenzyl)amino)methyl)benzoic acid (L_1)

The compound **L'$_1$**(1.5 g, 3.5 mmol) was added to compound **4** (1.7 g, 3.3 mmol) together with K_2CO_3 (1.0 g, 7.25 mmol) and KI (0.5 g, 3.0 mmol) dissolved in CH_3CN. The resultant solution was refluxed for 48 hrs, and the solvent was removed by rotary evaporation. The residue was dissolved and purified in SiO_2 with CH_2Cl_2 and CH_3OH (60:40) (R_f =0.59) to obtain compound **5**. LiOH (0.91 g, 3.8 mmol) was added to compound **5** (2.4 g, 2.55 mmol) dissolved in THF (5 ml) and kept at RT for 18 hrs. The solvents were evaporated in vacuo to obtain L_3. Compound L_3 (2.0 g, 2.45 mmol) was dissolved in CH_2Cl_2 was dissolved in TFA (50 ml) and stirred for 6 hrs, and the solvent was evaporated to obtain L_1 (1.5 g, 2.0 mmol, 95 % yield). The products L_3 and L_1 were purified with preparative HPLC.

For L3,
^{1}H NMR (400 MHz, MeOD, TMS): δ 2.83 (24 H, m, br, macrocycle C<u>H</u>$_2$,2H, s,br, NHC<u>H</u>$_2$CH$_2$CO, 2H, s, NHCH$_2$C<u>H</u>$_2$NH), 3.25 (2H, s, NHC<u>H</u>$_2$CO) , 3.91 (4H, s, NC<u>H</u>$_2$Ph) , 4.25 (6H, s, COOC<u>H</u>$_3$), 7.33 (8H, d, <u>H</u>Ph)
^{13}C NMR (400 MHz, MeOD, TMS): δ 34.12 (NH<u>C</u>H$_2$CH$_2$CO), 42.05(COO<u>C</u>H$_3$) 49.21 (macrocycle, <u>C</u>H$_2$), 51.83 (macrocycle, <u>C</u>H$_2$), 54.61 (NHCH$_2$<u>C</u>H$_2$CO), 57.10 (NHCH$_2$CO), 63.18 (N<u>C</u>H$_2$Ph), 129.44 (<u>C</u>HPh), 130. 62 (<u>C</u>HPh), 131.94 (<u>C</u>HPh), 135.76 (<u>C</u>HPh), 163.18 (Ph<u>C</u>OOH), 173.16 (macrocycle, <u>C</u>OOH)
MS(ESI-positive) m/z = 743.30 [M-H+] (calculated 742.35)

For L1,
^{1}H NMR (400 MHz, D$_2$O, TMS): δ 2.55 (24 H, m, br, macrocycle C<u>H</u>$_2$,2H, s,br, NHC<u>H</u>$_2$CH$_2$CO, 2H, s, NHCH$_2$C<u>H</u>$_2$NH), 3.25 (2H, s, NHC<u>H</u>$_2$CO) , 3.59 (4H, s, NC<u>H</u>$_2$Ph) , 7.33 (8H, d, <u>H</u>Ph)
^{13}C NMR (400 MHz, D$_2$O, TMS): δ 36.54 (NH<u>C</u>H$_2$CH$_2$CO), 50.82 (macrocycle, <u>C</u>H$_2$), 53.41 (NH<u>C</u>H$_2$<u>C</u>H$_2$CO), 56.13 (N<u>C</u>H$_2$Ph), 129.15 (<u>C</u>HPh), 130.00 (<u>C</u>HPh), 132.67 (<u>C</u>HPh), 167.54 (Ph<u>C</u>OOH), 171.26 (macrocycle, <u>C</u>OOH)
MS(ESI-positive) m/z = 715.10 [M-H$^+$] (calculated 714.32)

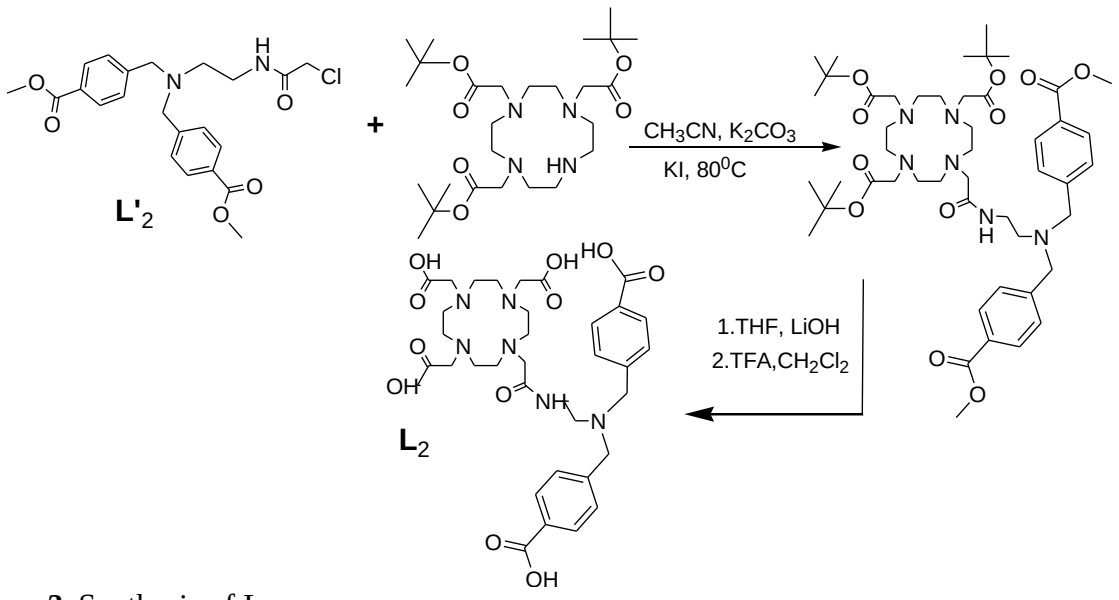

Scheme 3. Synthesis of L_2.

4-(((2-(((4,7-bis(carboxymethyl)-10-(3-hydroxy-2-oxopropyl)-1,4,7,10-tetraazacyclododecan-1-yl)acetyl)amino)ethyl)(4-carboxybenzyl)amino)methyl)benzoic acid (L_2)

The compound L'_2 was synthesized by using 4-Bromomethyl benzoic acid and Compound 1 following the same procedure as for L'_1. The compound L'_2 (1.5 g, 3.5 mmol) was dissolved in CH_3CN and followed the same synthesis procedure as in L_1 to obtain compound L_2 (1.1g, 1.5 mmol).

For L1,
^{1}H NMR (400 MHz, D_2O, TMS): δ 2.69 (24 H, m, br, macrocycle C$\underline{H}_2$,2H, s,br, NHC$\underline{H}_2$CH$_2$CO, 2H, s, NHCH$_2$C$\underline{H}_2$NH), 3.28 (2H, s, NHC$\underline{H}_2$CO) , 4.34 (4H, s, NC$\underline{H}_2$Ph) , 7.37 (8H, d, $\underline{H}$Ph)

^{13}C NMR (400 MHz, D_2O, TMS): δ 36.54 (NH$\underline{C}$H$_2$CH$_2$CO), 51.49 (macrocycle, $\underline{C}$H$_2$), 51.88 (macrocycle, $\underline{C}$H$_2$), 57.62 (NHCH$_2\underline{C}$H$_2$CO), 58.00 (NHCH$_2$CO), 61.20 (N$\underline{C}$H$_2$Ph), 128.89 ($\underline{C}$HPh), 130. 15 ($\underline{C}$HPh), 132.53 ($\underline{C}$HPh), 136.32 ($\underline{C}$HPh), 163.18 (Ph$\underline{C}$OOH), 173.16 (macrocycle, $\underline{C}$OOH)

MS(ESI-positive) m/z = 715.0 [M-H$^+$] (calculated 714.32)

2. General Procedure for preparation and characterization of lanthanide-ligand complexes

The ligand (L_1, L_2, and L_3) was dissolved in MilliQ grade water and mixed with a lanthanide chloride (Gd, La, Eu) in 5-10% excess stochiometric amount. The solution pH was adjusted to 6.0-6.5 by addition of NaOH and stirred at room temperature for 18 hrs. Unreacted Gd^{3+} was $Gd(OH)_3$ by raising the pH to 9.0 with the addition of 1 M NaOH. The crude residue was purified with preparative HPLC to obtain the Complex and characterized by LC-MS.

MS GdL_3 (ESI-positive) m/z = 898.10 [M-H$^+$] (calculated 897.05)

MS GdL_1 and GdL_2 (ESI-positive) m/z = 869.74 [M-H$^+$] (calculated 869.01)

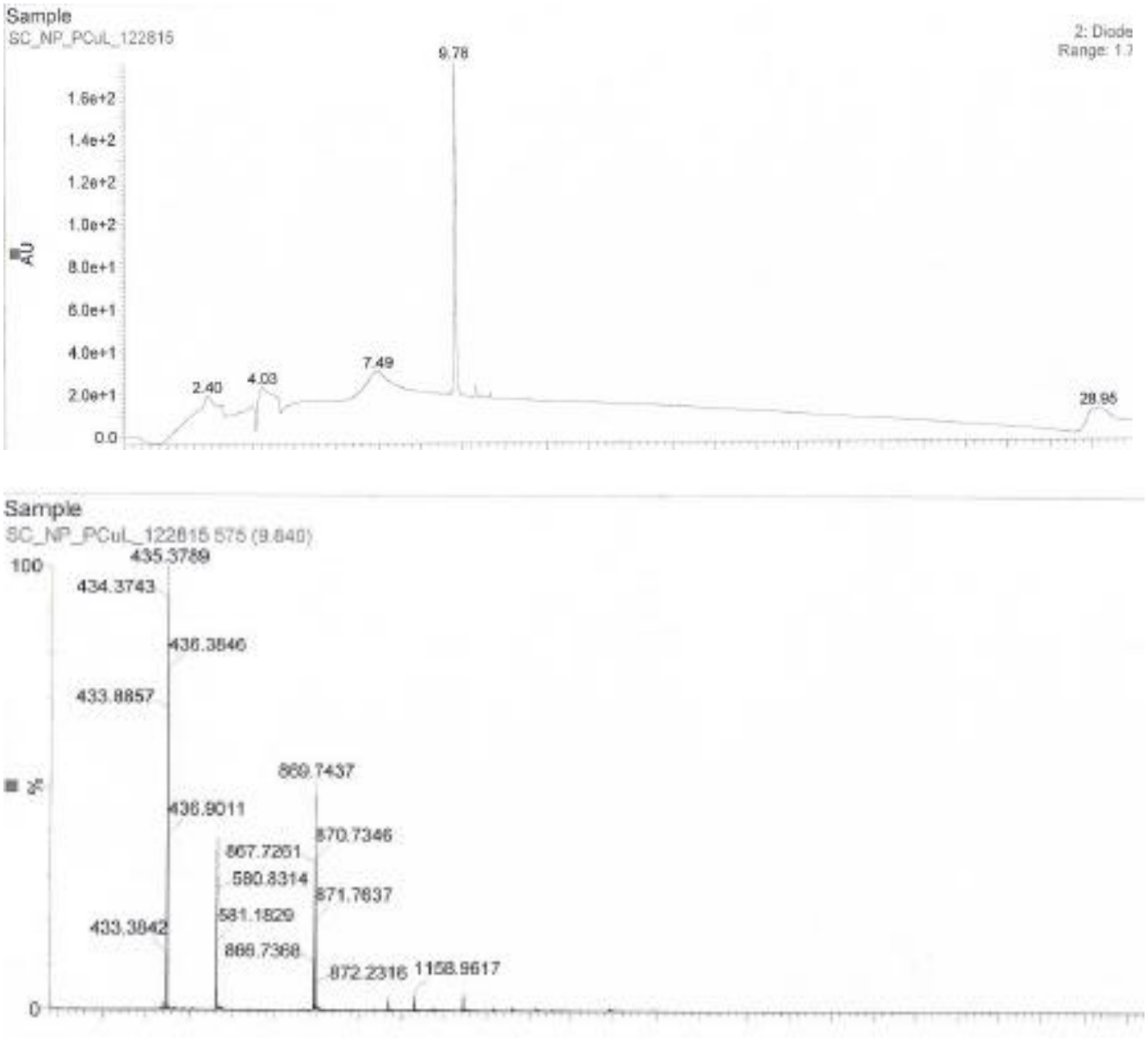

Figure S1. LC-MS of GdL_1 Complex

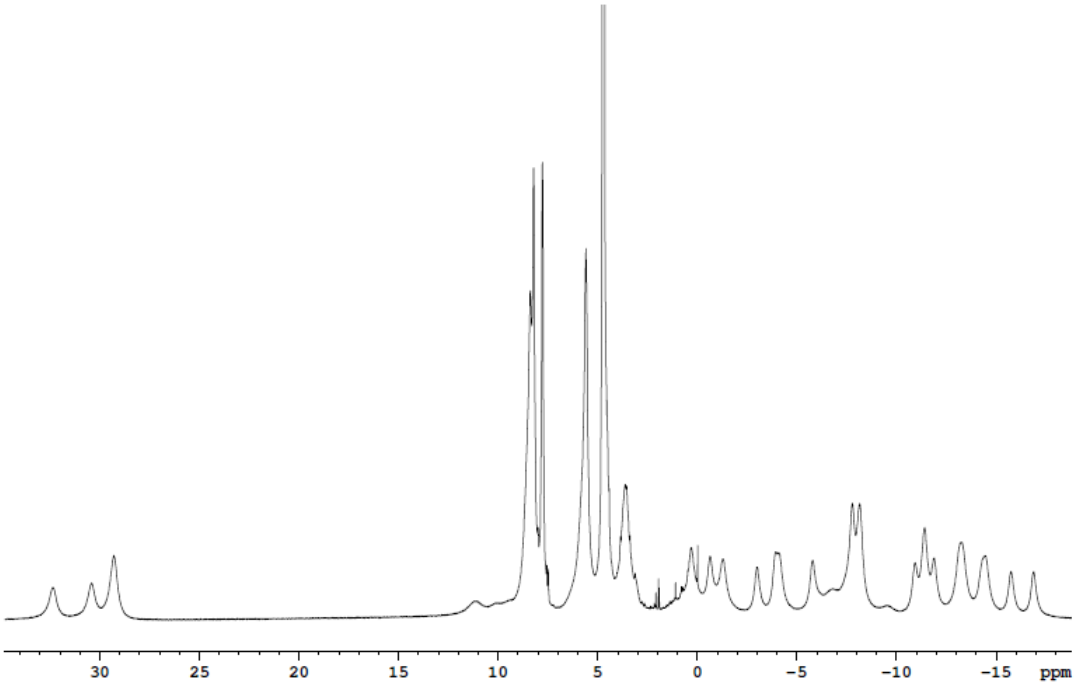

Figure S2. ^{1}H NMR spectrum of EuL_1 showing square antiprism (SAP) and twisted square antiprism (TSAP) structure in an approximate 4:1 ratio.

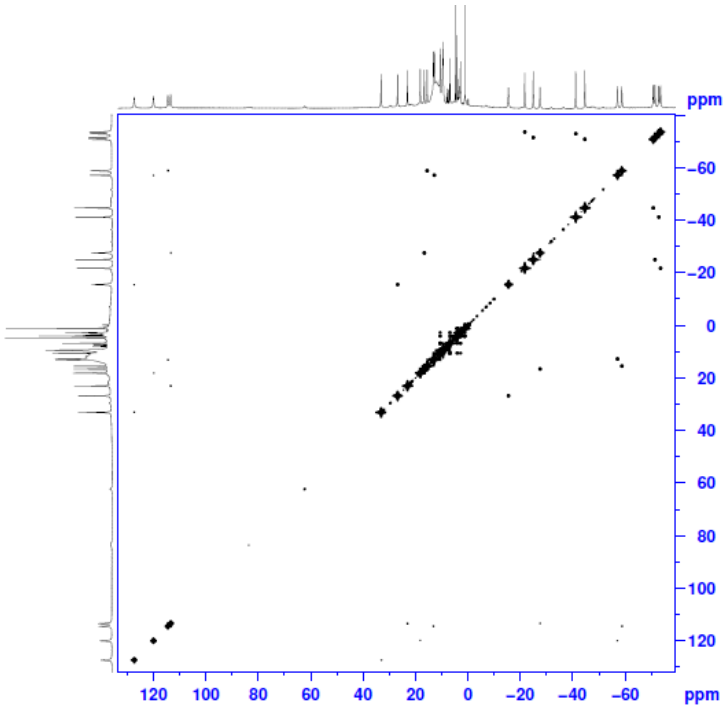

Figure S3. 2D-COSY spectrum of 80 mM YbL_1.

3. Relaxivity Measurements in the presence of Cations

Longitudinal relaxivity values were measured in MRS-6 NMR analyzer at 20 MHz and determined from the slope of the line of $1/T_1$ versus the concentration of gadolinium. Various solutions with different concentrations of GdLx complexes were prepared in 0.1 M MOPS buffer pH= 7.4 or buffer with 600 µM HSA. $CuCl_2$, $ZnCl_2$, $MgCl_2$ and $CaCl_2$ was then added to each of above complex solutions to obtain the desired [GdL]: $[M^{n+}]$ ratios for the titrations. After 30 min of incubation at 310 K, T_1 measurements were made at same temperature using warm air blown over the sample to maintain constant temperature. For relaxivity measurements with Cu^+, $[Cu(NCCH_3)_4]PF_6$ was dissolved in acetonitrile and the solution was diluted accordingly to obtain the final solution of GdL_1 that contain <2% in acetonitrile by volume. All the Cu^+ samples were prepared under anaerobic conditions. For relaxivity measurements with Fe^{3+}, $FeCl_3$ was dissolved in 0.1 M HCl for immediate use. The final solution of GdL_1 used in measurements contained <2% of this solution to avoid significant pH changes. MOPS buffer was used in all the measurements due to its weak interaction with Cu^{2+}.

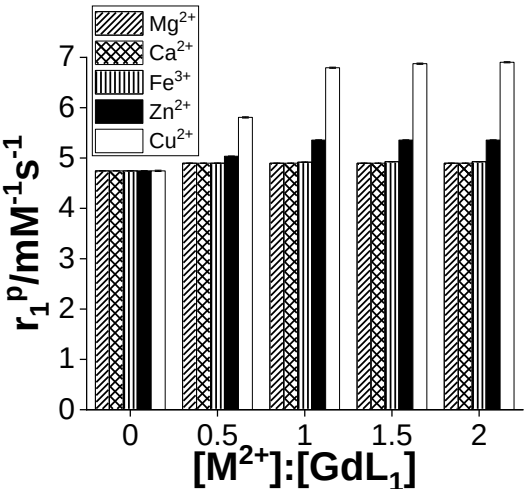

Figure S4. Relaxivity response of 0.5 mM GdL_1 to various metal ions in 0.1M MOPS buffer (pH 7.4) at 20 MHz and 37°C.

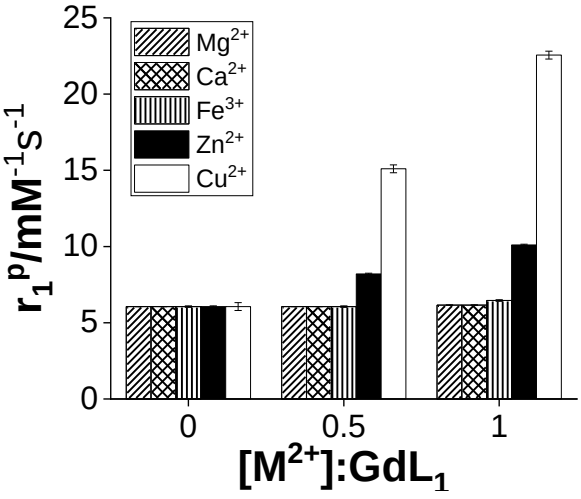

Figure S5. The r_1 relaxivity of 0.5 mM GdL_1 after addition of Mg^{2+}, Ca^{2+}, Fe^{3+}, Zn^{2+} or Cu^{2+} in 0.1M MOPS buffer (pH 7.4) and 600 µM HSA at 37°C and 20MHz.

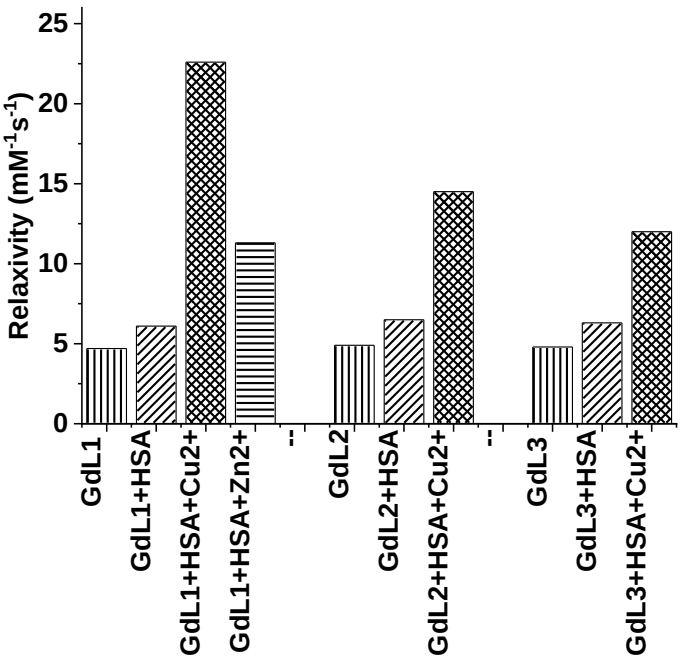

Figure S6. Relaxivity response of 0.5 mM GdL_{1-3} to 1 equivalent of Zn^{2+} and Cu^{2+} in 0.1M MOPS buffer (pH 7.4) with 600 µM HSA at 37ºC at a proton Larmor frequency of 20MHz.

4. Relaxivity Measurements in the presence of Anions

Longitudinal relaxivity values were measured in MRS-6 NMR analyzer at 20 MHz and determined from the slope of the line of $1/T_1$ versus the concentration of gadolinium. Relaxivity measurement performed for MOPS, PBS (20 mM and pH 7.3) lactate (2.3 mM), and HCO^{3-}(10 mM) in the presence of 0.5 mM GdL_1 and 0.5 mM Cu^{2+} in 0.1 M MOPS (pH 7.4) buffer at 37°C.

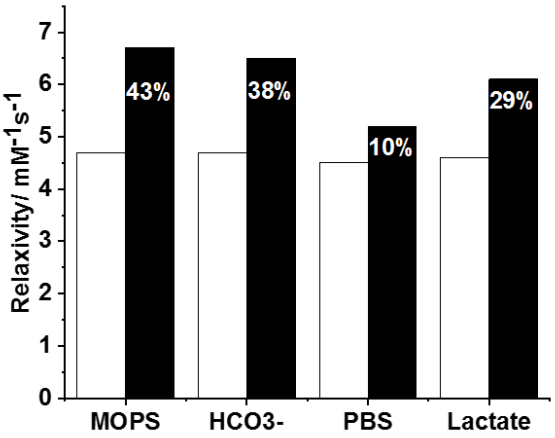

Figure S7. The relaxivity (r_1) of GdL_1 in the presence of various anions. The white bars represent the GdL_1 in the presence of various anions without Cu^{2+} ions. Black bars represent the relaxivity of GdL_1 with Cu^{2+} in the presence of different anions. Percentage values represents the % increase in relaxivity.

5. Relaxivity Measurements in the presence of Zn^{2+} ions

Longitudinal relaxivity values were measured in MRS-6 NMR analyzer at 20 MHz for various concentrations of Zn^{2+} (0.5, 1.25,2.5 and 5 mM) in the presence of 0.5 mM $GdL_1$and 0.5 mM Cu^{2+} in 0.1 M MOPS (pH 7.4) buffer at 37°C.

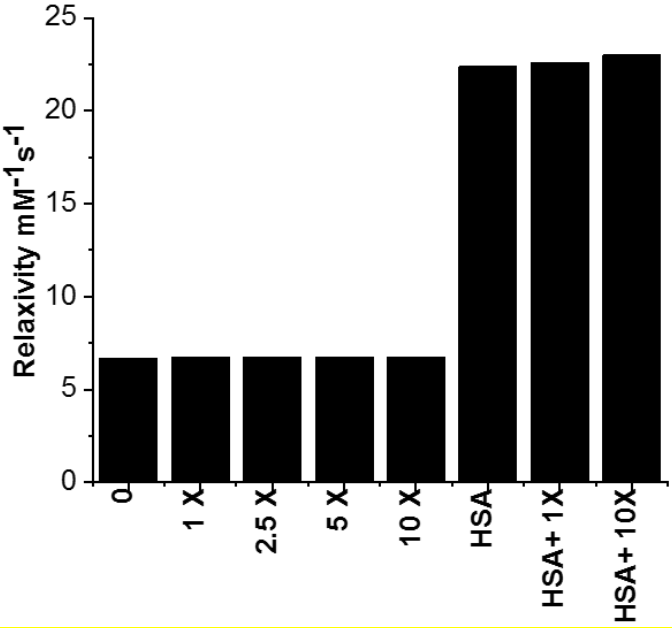

Figure S8. Relaxivity (r_1) of 0.5 mM GdL_1 with 0.5 mM Cu^{2+} in the presence of various concentration of Zn^{2+} (0.5, 1.25, 2.5 and 5 mM). Last three data bars represent the relaxivity (r_1) of 0.5 mM GdL_1 with 0.5mM Cu^{2+} in the presence of 0.6 mM HSA and various concentration of Zn^{2+} ions (0.5 and 5 mM).

6. Job's Plot

Ten samples of 500µl mixture of GdL_1 and Cu^{2+} were prepared with mole ratio varying from 1:9 to 9:1, while the total molar concentration of GdL_1 and Cu^{2+} kept constant at 0.2mM. The relaxivities of the samples were measure as at 20 MHz and 37°C as described above.

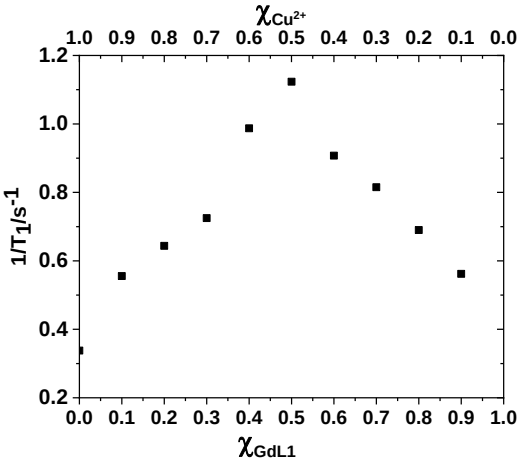

Figure S9. Job's plot for GdL_1 and Cu^{2+}.

7. Determination of the GdLx-Cu^{2+} binding constants by fluorescence

A 20-35 µM solution of GdL_{1-3} was prepared in 10mM Tris buffer (pH = 7.4) and titrated with 100 mM $CuCl_2$ stock solution. Addition of Cu^{2+} results in quenching of the native fluorescence of each GdL_{1-3} complex. The fluorescence intensity was measured upon each addition of Cu^{2+} at 25°C using a Fluoromax-4 Spectrofluorimeter in a 1cm quartz cuvette (Horiba). The excitation wavelength for all GdL sensors was at 260 nm. The emission wavelength for GdL_1 was 350 nm while the emission wavelength for GdL_2 and GdL_3 was 404 nm and 326 nm respectively. The GdL-Cu^{2+} dissociation constant was determined by fitting the data to the following equations.

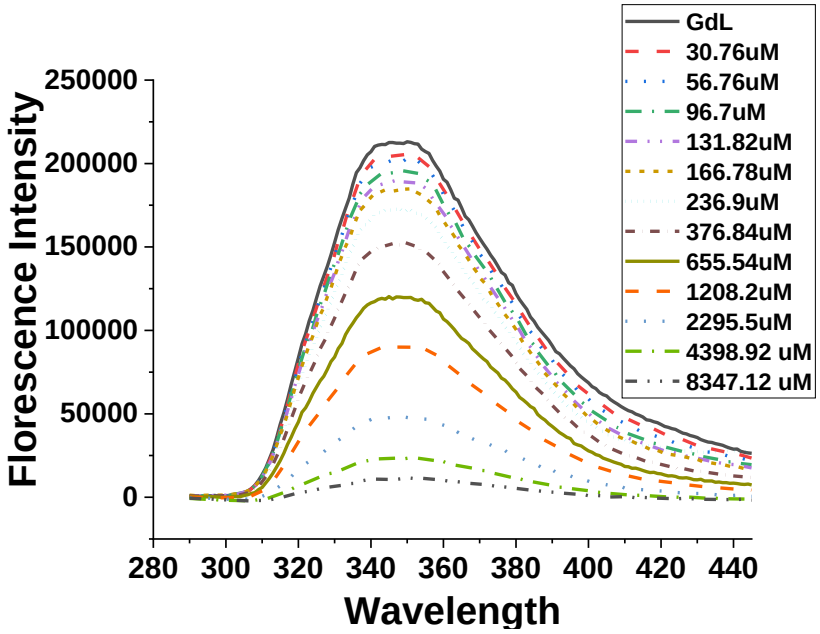

Figure S10. Florescence emission spectra for 20µM GdL_1 titrated in 0.1 M Tris Buffer.

$\Delta F = (\Delta F_{max}\,[Cu^{2+}]) / (K_d + [Cu^{2+}])$

$\Delta F = F_{GdL} - F_{GdL\text{-}Cu2+}$

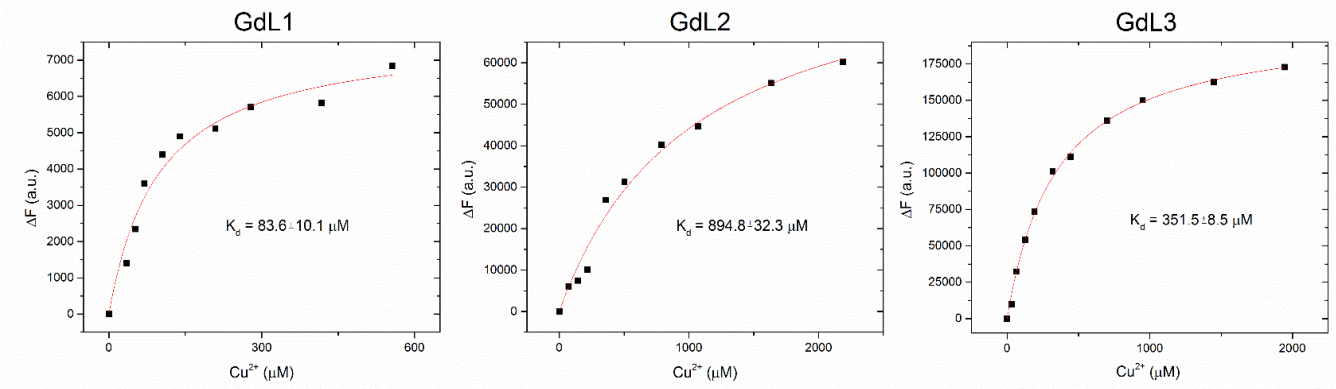

Figure S11. Experimental and fitted titration curves for change in fluorescence intensity upon titration with Cu^{2+} at 25°C for GdL_1, GdL_2, GdL_3.

8. Determination of Cu mediated ternary complex formation by Size-Exclusion Chromatography

Equimolar solutions (100 µM) of LaL_1: HSA: Cu^{2+}, LaL_1:Cu^{2+} and LaL_1: HSA were prepared and purified with size exclusion chromatography in Hi-trap desalting column (5 ml, 1.6 X 2.5 cm) using an FPLC (AKTA, GE HealthCare). Each collected peak was analyzed for La^{3+} ion concentration in 4% HNO_3 solutions using ICP-MS.

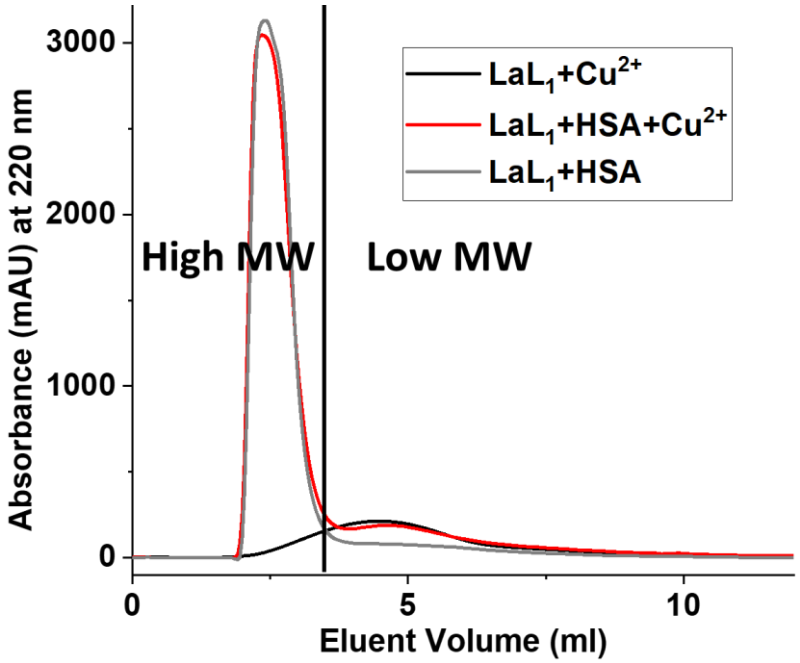

Figure S12. Chromatogram for of size exclusion chromatography

Table S1. Lanthanum metal ion concertation in high-molecular-weight fraction and low-molecular-weight fraction.

Sample	La^{3+} ion concentration in High MW fraction (µM)	La^{3+} ion concentration in Low MW fraction (µM)
LaL_1+Cu^{2+}	10	84
LaL_1+HSA+Cu^{2+}	63	28
LaL_1+HSA	14	82

9. Determination of the binding constants for GdL-Cu binding with HSA by relaxometry

The binding constants of each GdLx complex with HSA were determined by proton relaxation enhancement (PRE) measurements according to published procedures.[4,5] The proton relaxation rates were measured at increasing concentrations of protein using a MRS-6 NMR analyzer (20 MHz, 310 K). For the E-titration, the concentrations of each GdLx

complex (0.1 mM) and Cu^{2+} (0.1 mM) were kept constant, while HSA concentration was varied from 0 to 0.7 mM. ([GdLx]: [Cu^{2+}] = 1:1)

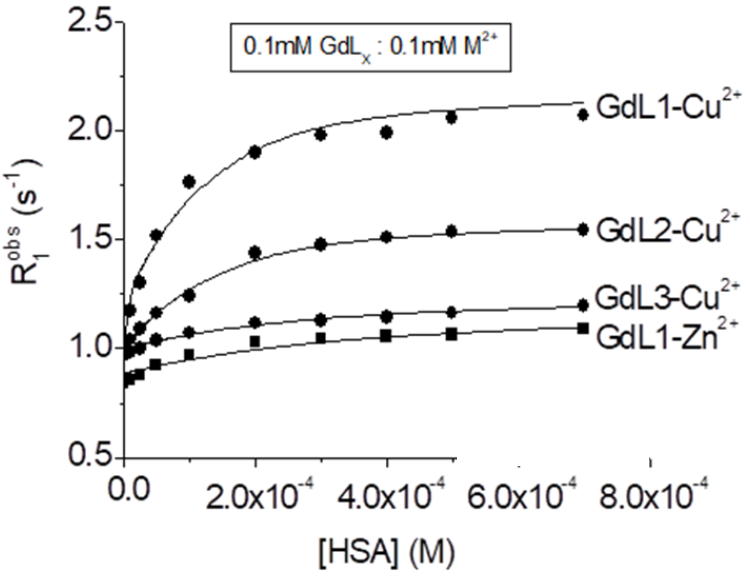

Figure S13. Proton relaxation enhancement of GdL_{1-3}-Cu^{2+}/Zn^{2+} complexes with increasing concentration of HSA. All measurements were performed at 20 MHz and 310 K in 0.1 M MOPS buffer at pH 7.4.

Table S2. Best-fit parameters relaxivity and K_d values for GdL_{1-3} in 0.1 M MOPS buffer (pH 7.4) at 37ºC.

Gd-Complex	**GdL_1**		**GdL_2**	**GdL_3**
Metal	**Cu^{2+}**	**Zn^{2+}**	**Cu^{2+}**	**Cu^{2+}**
K_d (µM)	44.0 ± 3	110 ± 20	59± 5	60 ± 10
r_1 ($mM^{-1}.s^{-1}$)	22 ± 0.5	11 ± 0.9	17 ± 0.6	12.9 ± 0.8

10. ^{17}O NMR measurements

^{17}O NMR experiments were performed at 9.4 T on a Bruker AVANCE III NMR spectrometer and temperature was regulated by air flow controlled by a Bruker VT unit. The samples ([Gd^{3+}] = 25.4 mM) were prepared in ^{17}O enriched water (10%) with the pH being maintained at 7.4 with 0.1 M Tris buffer. The sample was loaded into 80 µL spherical bulb (Wilmad-Lab Glass, Vineland, NJ) and placed inside a 5 mm NMR tube. Longitudinal relaxation rates ($1/T_1$) were obtained by the inversion recovery method, and transverse relaxation rates ($1/T_2$) were obtained

by the Carr–Purcell–Meiboom–Gill spin echo technique. Acidified water (pH = 3.0) containing 10% enriched ^{17}O water was used as a reference for the measurements. The corresponding fittings were performed with the Scientist 3.0 software (Micromath®). ^{17}O NMR data have been analyzed within the framework of Solomon-Bloembergen-Morgan theory as previously reported.[6]

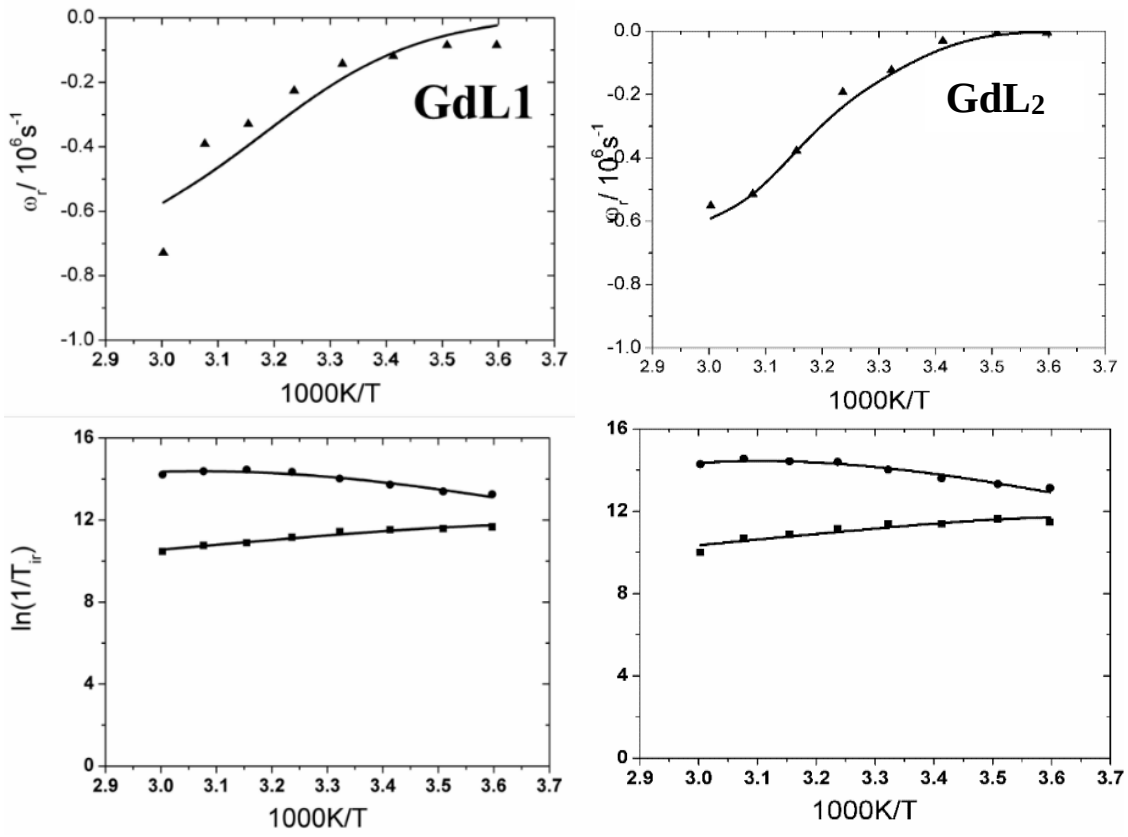

Figure S14. Temperature dependence of the reduced longitudinal (■) and transverse (▲) ^{17}O relaxation rates and reduced chemical shifts (●) of the GdL1(25.4 mM) and GdL2 (25.1 mM) in aqueous solution B_0= 9.4 T.

The longitudinal relaxivity (r_1) of Gd-complexes such as this is governed by several parameters including the water exchange rate (k_{ex}), the number of inner-sphere water molecules on Gd^{3+} (q), and rotational tumbling of the molecule (τ_R) (see equations in supporting information). A simple and direct way to measure the water exchange rate is by measuring the temperature-dependent T_{2s} by ^{17}O NMR (Figure S14). A fit of those T_2 data to theory gave the water exchange rates reported in Table S3. Both the GdL_1 and GdL_2 had similar water exchange rates (k_{ex}), somewhat slower than that reported for GdDOTA (k_{ex} = ~ 3 X 10^6 s^{-1}) as expected for monoamide derivatives.[7] The number of the inner-sphere bound waters (q) coordinated to Gd^{3+} in these complexes was also calculated q ~1.0 ± 0.2 for all complexes by the Evans method.[8-12] Underlined values has been fixed in the fitting.

Table S3. Best-fit parameters obtained for GdL_1 and GdL_2 from analysis of ^{17}O NMR data.

Parameters	GdL_1	GdL_2	GdDOTA
r_1 [$mM^{-1} s^{-1}$] 20MHz	4.7±0.1	4.9±0.1	3.9
k_{ex}^{298} [$10^6 s^{-1}$]	2.0±0.3	1.9±0.3	4.1
t_m [ns]	497±1	526±1	243
$DH^{\ddagger}$ [kJ/mol]	40±5.0	45±7.0	49.8
E_R [kJ/mol]	18.0	18.0	16.1
t_{RO}^{298} [ps]	530±10	497±10	77
E_V [kJ/mol]	1.0	1.0	1.0
t_V^{298} [ps]	3.4	3.4	11
D^2 [$10^{20} s^{-2}$]	0.55	0.55	0.16
A/ħ [$MHz/10^{-6}$]	-3.9±0.3	-3.9±0.2	-3.7

11. Kinetic Testing

Kinetic inertness was determined according to the published procedure with some modifications.[13,14] A sample containing 30mM phosphate buffer with 1.5 mM GdL_1 and 4.5 mM of $CuCl_2$ was used to record the decrease in R_1 value upon transmetallation with zinc (Due to the transmetallation, Gd^{3+} ions should forms phosphonate species that is insoluble in water and precipitate) . The T_1 of samples was measured 15 minutes after the stabilization of sample temperature at 310 K on 20 MHz NMR analyzer over the time.

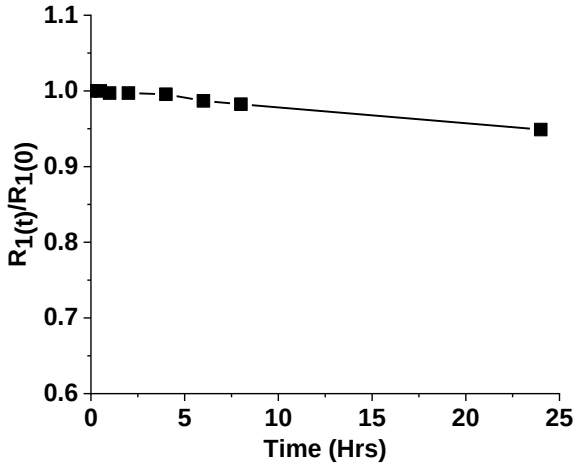

Figure S15. Relaxivity measurements of 1.5 mM GdL_1 and 4.5 mM Cu^{2+} in 30 mM Phosphate buffer in 310 K at 20 MHz.

12. Electrochemistry

Cyclic voltammograms were obtained with a CV50-W electrochemical analyzer using a glassy carbon working electrode, an Ag/AgCl reference electrode and a platinum wire auxiliary electrode. Samples were prepared in 0.1M MOPS under N_2 and analyzed using a scan rate of 100 mV/s. $E_{1/2}$ values were the averages of E_{pa} and E_{pc}. GdL_1-Cu^{2+} quasi-reversible signal with oxidation peak at 0.31V and reduction peak at 0.01 V with a $E_{1/2}$ = 0.16V. This redox potential is consistent with selective binding of GdL_1 with Cu^{2+}.[15]

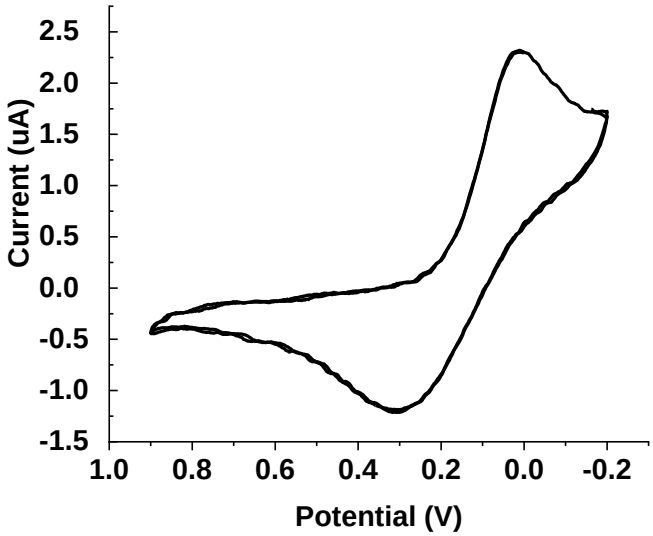

Figure S16. Cyclic voltammograms of GdL_1 acquired in 0.1 M MOPS buffer (pH 7.4) at 25 °C. All potentials are referenced to the standard hydrogen electrode (SHE).

13. Determination of GdL_1-Cu coordination by ^{1}H-NMR

To learn more about the binding interactions between Cu^{2+} and GdL_1, high-resolution ^{1}H NMR spectra of LaL_1 (the diamagnetic analog) were recorded in D_2O before and after addition of $CuCl_2$. 20 mM solution of $LaL_1$was prepared and titrated with various concentrations (1,10,15,20,25 and 40 mM) of Cu^{2+}. The ^{1}H NMR or LaL_1 was recorded at 37°C with Bruker AVANCE III 400 MHz NMR spectrometer. The ^{1}H NMR signals corresponding to the phenyl ring of benzoic acid (H_a, H_b, H_c, and H_d) and the H_e and H_f methylene protons in the spectrum of LaL_1 broadened and shifted upon addition of Cu^{2+} (Figure S17). Although one sees broadening of the benzoic acid protons and the H_e protons near the tertiary amine consistent with Cu^{2+} coordination near those groups,[16-18] we also observe the general broadening in the aliphatic region, so the NMR data alone does not allow us to draw any definitive conclusions about the Cu^{2+} binding site.

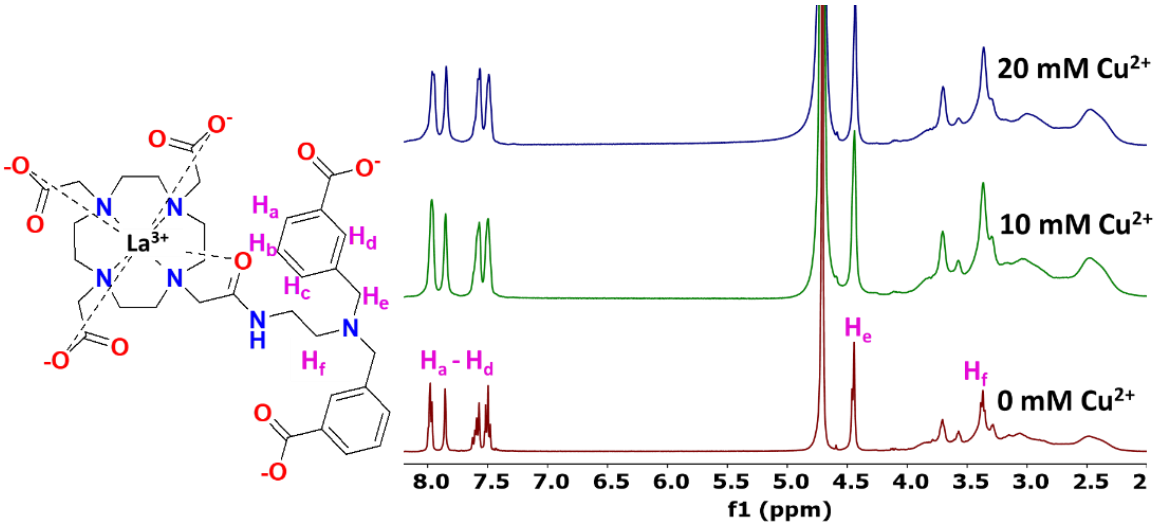

Figure S17. ^{1}H NMR titration spectra of 20 mM LaL_1 in the presence of various concentrations of Cu^{2+}at 37°C in D_2O.

14.EPR

Equimolar solutions (250 µM) of LaL_1: HSA: Cu^{2+}, LaL_1:Cu^{2+} and Cu^{2+}: HSA were prepared in 10mM MOPS buffer at pH 7.2. All the EPR spectra were obtained at 30K Bruker EMX Spectrometer operating at a microwave frequency of ~ 9.3 GHz. The spectra were recorded at 10 K employing a helium flow cryostat, using a microwave power of 12.8 mW and a modulation amplitude of 10 Gauss.

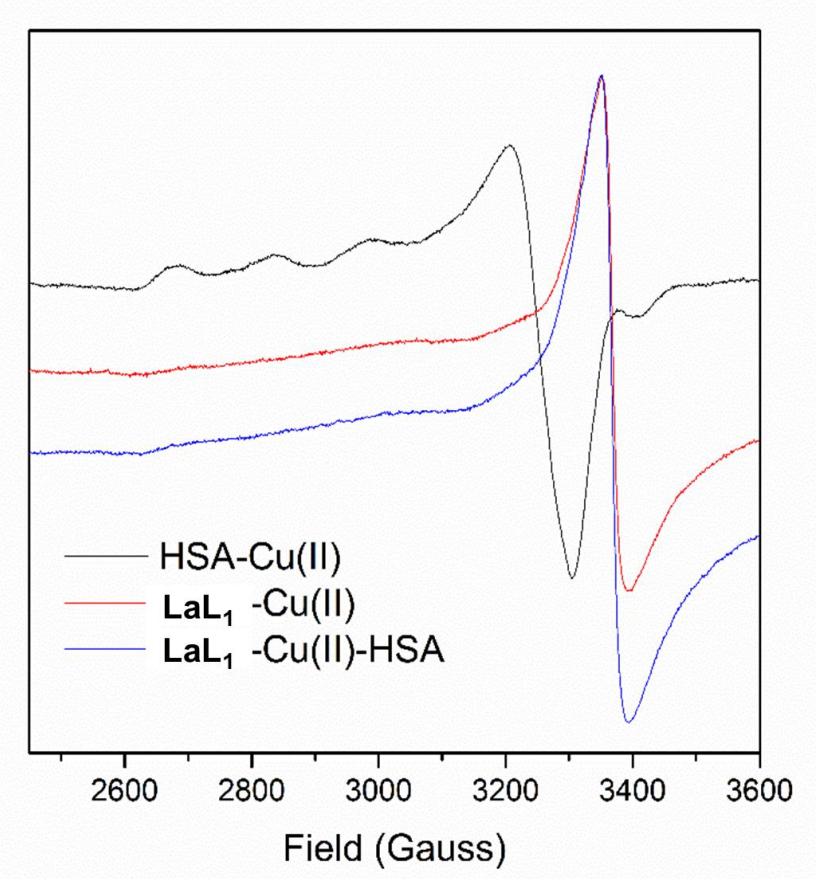

Figure S18. X-Band EPR Spectra of 250µM Cu^{2+} with 250uM LaL_1 in 250uM HSA in 10mM MOPS buffer at pH 7.2 (2,500–3,500 G, 9.3 GHz, 30K)

15. XAS (XANES and EXAFS)

GdL_1-Cu^{2+}, HSA-Cu^{2+} and GdL_1-Cu^{2+}-HSA (2mM) in 20 mM MOPS pH 7, 10 % (w/v) glycerol were generated by addition of a $CuCl_2$ stock solution to GdL_1 and/or HSA and loaded into custom made polycarbonate XAS sample cells, sealed with tape, flash frozen in liquid nitrogen and stored in liquid nitrogen until data collection. X-ray absorption spectroscopy measurements were performed at Stanford Synchrotron Radiation Lightsource with the SPEAR 3 storage ring.

Copper K-edge data were collected using beamline 9-3 with a wiggler field of 2 Tesla and employing a Si(220) double-crystal monochromator and a vertically-collimating pre-monochromator mirror. The incident and transmitted X-ray intensities were monitored using nitrogen-filled ionization chambers, and X-ray absorption was measured as the copper Kα fluorescence using a Lytle detector.

Nickel filters were placed between the cryostat and detector to reduce scattered X-ray not associated with Cu fluorescence. During data collection, samples were maintained at a temperature of ~10 K using an Oxford instruments liquid helium flow cryostat. XAS

spectra were measured using 10 eV steps in the pre-edge region (8750–8960 eV), 0.35 eV steps in the edge region (8960– 9010 eV) and 0.05 Å − 1 increments in the EXAFS region (to k = 13 Å $^{-1}$). Three to four scans were accumulated, and the energy was calibrated by reference to the absorption of a standard copper metal foil measured simultaneously with each scan, assuming a lowest energy inflection point of the copper foil to be 8980.3 eV. The cryostat was moved after each scan to prevent photoreduction and to have the X-ray beam focused on a new area of the sample holder where the sample was not exposed previously to radiation.

The extended x-ray absorption fine structure (EXAFS) oscillations (k) were quantitatively analyzed by curve fitting using the EXAFSPAK suite. Ab initio theoretical phase and amplitude functions were calculated using the program FEFF version 8.2.[19]

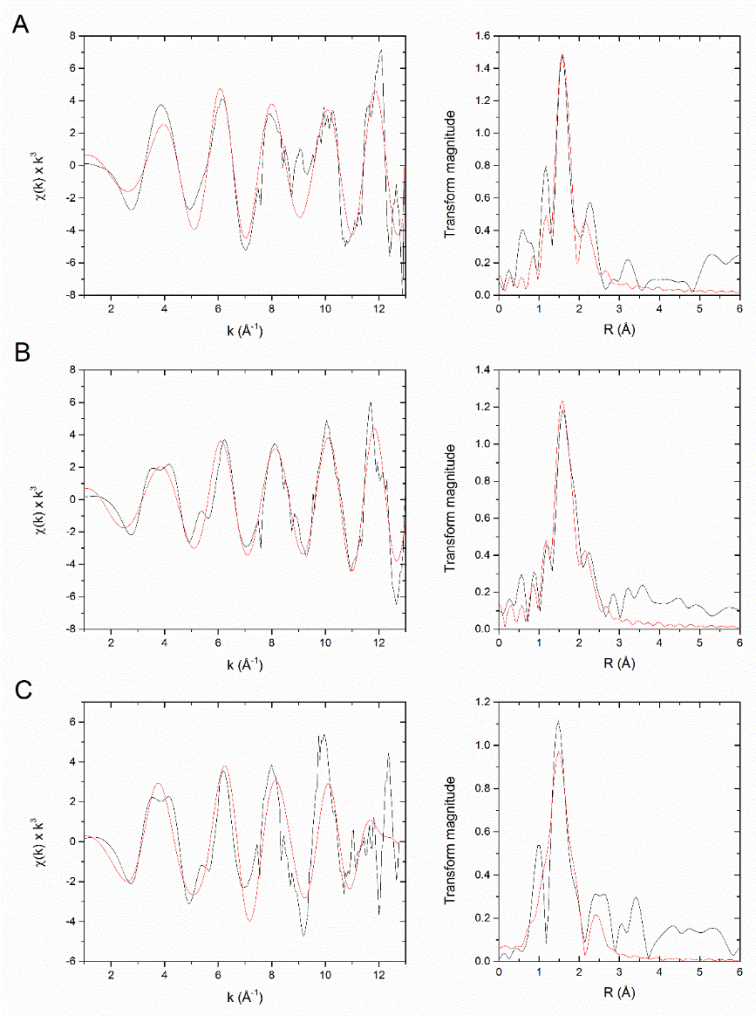

Figure S19. EXAFS experimental oscillations (black lines) and corresponding calculated best fits (red lines) and corresponding EXAFS Fourier transforms determined for GdL_1-Cu^{2+} (A), HSA-Cu^{2+} (B) and GdL_1-Cu^{2+}-HSA (C).

16. Molecular Modelling

The initial model of HSA at N-terminus site bound to Cu^{2+} was based on the published crystal structure of Cu bound DAHK (CCDC- 809109) that was determined by the crystal structures. The N-terminus site was imported into Hyperchem™7.5 (Hypercube, Inc.,) and previously optimized SAP conformation GdL_1 complex used in all coordination. Geometry optimization was performed based on EXAFS experimental bond lengths of N and O coordinated to the Cu centers. All optimizations were carried out using the Polak-Ribiere algorithm until the termination condition of 0.1 Kcal/(Å mol) RMS gradient was met.

17. In-vivo mouse imaging at 4.7T

All animal experiments were performed by guidelines set by the UT Southwestern Institutional Animal Care and Use Committee (IACUC). Male C57BL/6 mice were anesthetized with isofluorane. Once the animals were secured inside a 38-mm volume coil, the liver was positioned in the center of the 4.7 T Varian MRI scanner. Two 3D T1-weighted gradient echo pre-injection scans were obtained (TE/TR = 1.57/3.11 ms, NEX8, Matrix = 128 × 128 × 128). 0.1 mmol/kg of GdL_1/Gadavist/Multihance were injected to the mice after with and without injection of ATN-224 (n=3 for each group), and post-injection scans were obtained. Consecutive 3D T1-weighted scans were obtained sequentially to monitor signal enhancement in the liver over time. The slice selection of liver tissue was made by avoiding any bowel involvement in the slice. This resulted in slice selections encompassing the median and left lobes of the mouse liver. The images were quantified and analyzed using ImageJ (National Institutes of Health, Bethesda, MD). The signal intensities from ROIs of the liver were measured separately and averaged at 6, 9, 12, 15, and 18 minutes for GdL_1 and Gadavist. For the Multihance, signal intensities from ROIs of liver were measured and averaged at 4, 7, 10, 13, 16, 19, 23, 26, 29 and 32 minutes. The values were normalized to the signal intensity obtained from mouse back muscle. Contrast enhancement was calculated using the formula $\left(\frac{Signal\ post-injection}{Signal\ pre-injection} - 1\right) \times 100\%$. Statistical analysis was performed by comparing the mean values using a two-tailed *t*-test. P-values <0.05 were considered statistically significant.

18. Bio-distribution analysis of metal by ICP-MS

Mice were treated with GdL_1 and ATN-224 similar to the *in vivo* imaging experiments. After 5 min of injection of GdL_1, the mice were heavily anesthetized, and tissues were isolated. The tissues were homogenized and completely lysed in 2 ml freshly made aqua regia for 24 hrs. The samples were then heated at 120°C in an oil bath until complete evaporation of aqua regia. The residue was re-dissolved in 0.5M HCl and sonicated for 30 min. The samples were centrifuged at 4000 g for 5 min to eliminate any residue. The resultant samples were diluted with 4% HNO_3 and analyzed by ICP-MS.

References

1. Hu, H.; Lim, N.; Ding-Pfennigdorff, D.; Saas, J.; Wendt, K.U.; Ritzeler, O.; Nagase, H.; Pletenburg, O.;Schultz, C.; Nazare, M. DOTAM derivatives as active cartilage-targeting drug carriers for the treatment of osteoarthritis. *Bioconjugate Chemistry* **2015** *26* (3), 383-388.
2. ChemAxon – Software for Chemistry and Biology https://www.chemaxon.com/ (accessed June 15, 2017).
3. Kiyose, K.; Kojima, H.; Urano, Y.; Nagano, T. Development of a Ratiometric Fluorescent Zinc Ion Probe in Near-Infrared Region, Based on Tricarbocyanine Chromophore. *J. Am. Chem. Soc*. **2006**, 128, 6548–6549.
4. Martins, A. F.; Morfin, J.-F.; Geraldes, C. F. G. C.; Tóth, É. Gd(3+) complexes conjugated to Pittsburgh compound B: potential MRI markers of β-amyloid plaques**.** *J. Biol. Inorg. Chem*. **2013**, 19, 281–295.
5. Martins, A. F.; Morfin, J.-F.; Kubíčková, A.; Kubíček, V.; Buron, F.; Suzenet, F.; Salerno, M.; Lazar, A. N.; Duyckaerts, C.; Arlicot, N.; Guilloteau, D.; Geraldes, C. F. G. C.; Tóth, É. PiB-Conjugated, Metal-Based Imaging Probes: Multimodal Approaches for the Visualization of β-Amyloid Plaques. *ACS Med. Chem. Lett*. **2013**, 5, 436–440. Direct high-performance liquid chromatographic resolution of the enantiomers of tiaprofenic acid using immobilized human serum albumin. J. Pharm. Pharmacol. 1994, 46, 300-304.
6. Yu, J.; Martins, A.F.; Preihs, C.; Clavijo-Jordan,V.; Chirayil, S.; Zhao, P.; Wu, Y.; Nasr, K.; Kiefer, G.E.; Sherry, A.D. Amplifying the Sensitivity of Zinc(II) Responsive MRI Contrast Agents by Altering Water Exchange Rates. *J. Am. Chem. Soc.*, **2015**, 137, 44, 14173–14179.
7. Silverio, S.; Torres, S.; Martins, A. F.; Martins, J. A.; Andre, J. P.; Helm, L.; Prata, M. I. M.; Santos, A. C.; Geraldes, C. F. G. C. Lanthanide chelates of (bis)-hydroxymethylsubstituted DTTA with potential application as contrast agents in magnetic resonance imaging. *Dalton Trans*. **2009**, 24, 4656–4670.
8. Sherry, A.D.; Wu, Y. The importance of water exchange rates in the design of responsive agents for MRI. Curr. Opin, Chem, Biol. 2013, 17, 167-174.
9. Gonzalez, G.;Powell, D.H.; Tissieres, V.; Merbarch, A.E. Water-exchange, electronic relaxation, and rotational dynamics of the MRI contrast agent [Gd(DTPA-BMA)(H2O)] in aqueous solution: a variable pressure, temperature, and magnetic field oxygen-17 NMR study. J. Phys. Chem. 1994,98,53-59.
10. Aime, S.; Botta, M.; Fasano, M.; Crich, S.G.; Terreno, E. 1H and 17O-NMR relaxometric investigations of paramagnetic contrast agents for MRI. Clues for higher relaxivities. Coord. Chem. Rev. 1999, 321-333.
11. Caravan, P.; Farrar, C.T.; Frullano, L.; Uppal. R. Influence of molecular parameters and increasing magnetic field strength on relaxivity of gadolinium- and manganese-based T1 contrast agents. Contrast Media Mol. Imaging. 2009,4, 89-100.
12. Merbach, A.E.; Helm, L.; Toth, E., The Chemistry of Contrast Agents in Medical Magnetic Resonance Imaging, John Wiley & Sons, 2013.
13. Laurent, S.; Vander Elst, L.; Henoumont, C.; Muller, R. N. How to measure the transmetallation of a gadolinium complex. *Contrast Media Mol. Imaging* **2010**, 5, 305–308.
14. Jiang, D.; Min, L.; Wang, J.; hang, Y.; Chickenyun, S.; Wang, Y.; Zhou,F. Redox Reactions of Copper Complexes Formed with Different β-Amyloid Peptides and Their Neuropathalogical Relevance, *Biochemistry*, **2007**, 46, 9270-9282.
15. Chuquing, C.; Santos, O.; Xu, X.; Canarg, J.W. Synthesis and Cyclic Voltammetry Studies of Copper Complexes of Bromo- and Alkoxyphenyl-Substituted Derivatives of Tris(2-

pyridylmethyl)amine: Influence of Cation−Alkoxy Interactions on Copper Redox Potentials. *Inorg. Chem*., **1997**, 36, 1967-1972.
16. Mukherjee, P.; Drew, M.G.B.; Ghosh, A. Anion-Directed Template Synthesis and Hydrolysis of Mono-Condensed Schiff Base of 1,3-Pentanediamine and o-Hydroxyacetophenone in NiII and CuII Complexes. Eur. J.Inorg.Chem. 2008, 3372-3381.
17. Mouni, L.; Akkurt, M.; Yildrim, S.O.; Hadda, T.B.; Chohan, Z.H. Crystal Structure of Cuprate (II) Complex of Tetradentate ONNO Ligand: 4-[(2-{[(1E)-1-Methyl-3oxobtyldene]amino} ethyl) imino]pentan-2-one. J. Chem. Crystallogr. 2010, 40, 169- 172.
18. Karabiyik, H.; Erdem, O.; Aygun, M. Ligand-to-Metal Charge Transfer Resulting in Metalloaromaticity of [R,R-Cyclohexyl-1,2-bis(2-Oxidonaphthylideneiminato-N,N′,O,O′)]Cu(II): A Scrutinized Structural Investigation. J. Inorg. Organomet. Polym, 2010, 20, 142-145.
19. George, G.N., http://ssrl.slac.stanford.edu/exafspak.html.